Supplementary Information

A reversible fluorescent probe for hypochloric acid in living cells and animals: utilizing a novel strategy for effectively modulating the fluorescence of selenide and selenoxide

Zhangrong Lou[a,b] , Peng Li[a], Qiang Pan[a , b] and Keli Han*[a]

[a]State Key Laboratory of Molecular Reaction Dynamics, Dalian Institute of Chemical Physics (DICP), Chinese Academy of Sciences (CAS), 457 Zhongshan Road, Dalian 116023, P. R. China E-mail: klhan@dicp.ac.cn
[b] Graduate School of Chinese Academy of Sciences, Beijing 100049, China

Contents:

1. General Experimental Section

Materials and Characterization: The $ONOO^-$ source was the donor 3-Morpholinosydnonimine hydrochloride (SIN-1, 50.0 μmol/ml)[1]. NO is generated in form of 3-(Aminopropyl)-1-hydroxy-3-isopropyl-2-oxo-1-triazene (NOC-5). $^1O_2$ was generated by the reaction of H_2O_2 with NaOCl[2] and $O_2^-\cdot$ was created by KO_2[3]. ·OH was generated by Fenton reaction between Fe^{II}(EDTA) and H_2O_2 quantitively, and Fe^{II}(EDTA) concentrations represented ·OH concentrations[4]. Tert-butylhydroperoxide (t-BuOOH) and cumene hydroperoxide (CuOOH) could also use to induce ROS in biological systems[5]. Hypochlorous acid (HOCl) was standardized ($\varepsilon_{292\ nm}$= 350 $M^{-1}cm^{-1}$)[6]. 100 mM NaHS stock solution in Ultrapure water. Common reagents or materials were obtained from commercial source of analytical reagent grade, and used without further purification except as otherwise noted. Ultrapure water was used throughout the analytical experiments. ^{1}H NMR, ^{13}C NMR and ^{77}Se NMR spectra were obtained on a Bruker DRX-400 spectrometer, and the ^{1}H NMR and ^{13}C NMR chemical shifts (δ) are reported in ppm relative to TMS (Me_4Si) as internal reference.

Absorption and Fluorescence Analysis. Steady-state UV/Vis spectra were measured at room temperature on a Lambda 35 UV-visible Spectrophotometer (Perkin-Elmer) with 1.0-cm quatz cells. Fluorescence emission spectra were obtained at room temperature on a Fluoromax-4 Spectrofluorometer (Horiba-Jobin Yvon), with a Xenon lamp and 1.0-cm quartz cells. With a pipette gun (Eppendorf), taking 30 μL of the probe NI-Se (N, N'-Dimethylformamide, 1.0 mM) and then the solution was diluted to 3.0 μM with 10ml 20 mM PB buffers, NaOCl was added. The mixture was equilibrated for 8 min before measurement. The concentration of NI-Se was 3.0 μM throughout the analysis experiments except that otherwise pointed out. The fluorescence intensity was measured with the excitation wavelength 450 nm, and the excitation and emission slits set to 2 and 2 nm, respectively.

Cell Culture and Confocal Imaging. Murine RAW264.7 macrophage cells (ATCC, USA) were maintained following protocols provided by the American Type Culture Collection. Cells were seeded at a density of 1×10^6 cells mL^{-1} for confocal imaging in RPMI 1640 Medium supplemented with 15% fetal bovine serum (FBS), $NaHCO_3$ (2 g/L), and 1% antibiotics (penicillin /streptomycin, 100 U/ml). Cultures were maintained at 37 °C under a humidified atmosphere containing 5% CO_2. The cells were subcultured by scraping and seeding on 35 mm × 12 mm glass bottom cell culture dishes according to the instructions from the manufacturer. Florescent images were acquired on a FV1000 confocal laser-scanning microscope (Olympus) with an objective lens (×40) except for co-stain images (× 60). The excitation wavelength was set to 405 nm and 488 nm for Hoechst33342 and NI-Se, respectively. Prior to imaging, the medium was removed. Cell imaging was carried out after washing cells with physiological saline (0.9 %) for three times.

MTT Assay. RAW264.7 cells (10^6 cell mL^{-1}) were dispersed within replicate 96-well microtiter plates to a total volume of 200 μL $well^{-1}$. Plates were maintained at 37 °C in a 5% CO2/95% air incubator for 4 h. RAW264.7 cells were then incubated for 24 h upon different concentrations probe of 10, 20, 40, 60, 80 and 100 μM respectively. MTT (Sigma) solution (5.0 mg mL^{-1}, PBS) was then added to each well. After 4 h, the remaining MTT solution was removed, and 200 μL of DMSO was added to each well to dissolve the formazan crystals. Absorbance was measured at 570 nm in a

TRITURUS microplate reader.

Fluorescence Imaging in Living Mice. The fluorescent images were acquired in a Maestro in-vivo imaging system (CRi). The mice (6-8 weaks) purchased from Experimental animal center of Dalian Medical University were given an intraperitoneal (i.p.) injection of LPS (1 mg in 400 μL saline). After 4 h, the mice were anesthetized by isoflurane in a flow of oxygen. Then, the mice were injected intraperitoneally with NI-Se (100 nmol). As a control, untreated mice (neither treated with LPS nor NI-Se) or unstimulated mice intraperitoneally injected only with NI-Se (100 nmol) were also prepared. 5 min later, the mice were imaged with an excitation filter 455 nm and an emission range = 500–740 nm. In group (c), an additional H_2S (4 μmol) was injected and the acquired images was shown in group (d).

Computational Methods. Calculations were performed using Gaussian 09 programs[7]. Density functional theory (DFT) and time-dependent density functional theory (TD-DFT) methods were carried out and the Becke's three–parameter hybrid exchange functional with Lee-Yang-Parr gradient-corrected correlation (B3LYP functional) was used as the method of choice. Triple-ξ valence quality with one set of polarization functions (TZVP) basis set was used for all calculations. The equilibrium geometries of the ground state were optimized using density functional theory (DFT) method. The vertical excited energies were calculated at optimized geometries using the TD-DFT method. The calculations considered the solvent effects to be performed in the presence of a solvent by placing the solute in a cavity within the solvent reaction field (SCRF). The conductor-like screening model (COSMO) is used in SCRF. Water was employed as solvent in all the calculations. All the local minima were confirmed by the absence of an imaginary mode in vibrational analysis calculations.

HPLC analysis. NI-Se and NI-SeO were separated on an Elite HPLC system equipped with UV-vis absorption detectors. 25 μL of sample was injected into the HPLC system equipped with a C_{18} column (Alltech, Kromasil, 250 mm × 4.6 mm, 5 μm) equilibrated with CH_3CN. The compounds were separated with CH_3CN:water = 95:5 using a flow rate of 1 mL/min. Under those conditions NI-Se eluted at 7.1 min, and NI-SeO at 2.8 min. The peak signals were detected by monitoring the absorption at 450 nm for NI-Se and 254 nm for NI-SeO.

2. Synthesis and Characterization of Compounds

The general synthetic route of the compound **NI-Se** was described in Scheme S1.

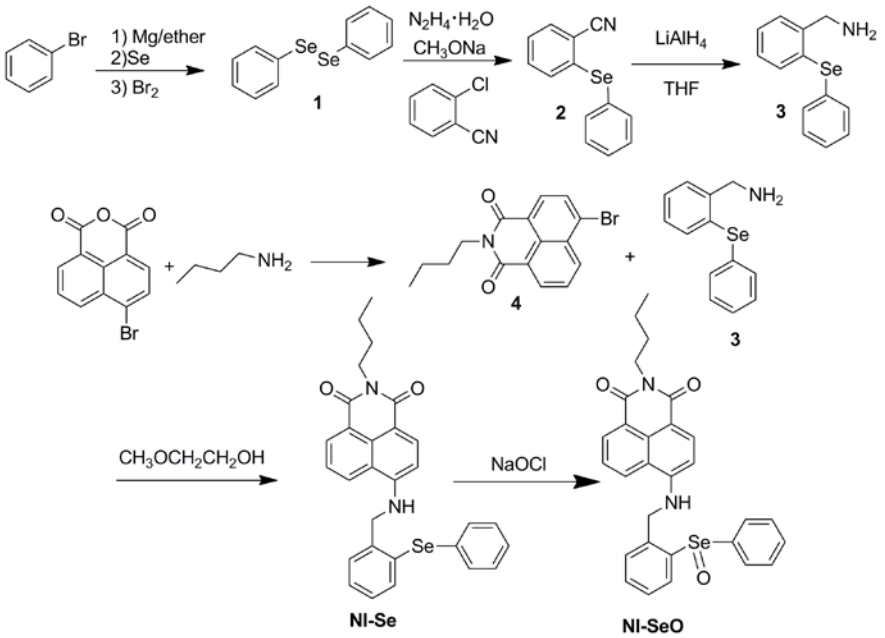

Scheme S1. The synthesis of compound NI-Se.

Synthesis of diphenyl diselenide (1). This compound was prepared according to a slight modification of the literature procedure[8]. Under the nitrogen atmosphere, to a three-neck flask containing 35 ml anhydrous diethyl ether suspended with 2.40 g (100 mmol) magnesium powder was dropped 15.70 g (100 mol) bromobenzene diethyl ether (10 ml) solution. After the phenylmagnesium bromide was prepared, the dropping funnel was instead of a straight considering pipe. Then 7.01 g (90 mmol) of selenium was added in portions at a rate sufficient to maintain a vigorous reflux through the straight considering pipe. The addition requires 15–30 minutes, after which the mixture was stirred and heated for another 40 minutes to ensure the selenium was dissolved completely. The residual Grignard reagent was hydrolyze with 0.30 g of water. After the generated solution was cooled to 5 °C with ice bath, 2.4 ml of bromine was added in drops at a rate such that the ether does not reflux. Cooling and stirring were continued as a solution of 5.35 g (100 mmol) of ammonium chloride in 29 ml of water was added slowly. The mixture was filtered, and the precipitate was washed thoroughly with ether. Then the combined filtrates were evaporated and the acquired coarse product was recrystallized with *n*-hexane, a yellow microcrystalline solid was obtained (4.97 g, 35.4%). ^{1}H NMR (400 MHz, $CDCl_3$) δ(ppm): 7.62-7.59 (m, 2H), 7.28-7.23 (m, 3H).

Synthesis of 2-(phenylselanyl)benzonitrile (2). This compound was prepared according to a slight modification of the literature procedure[9]. 1.24 ml of hydrazine hydrate and 16.00 g of 20 % methanol sodium methanol solution were added to a solution in a 250 ml three-neck flask containing 12.49 g (40 mmol) of diphenyl diselenide **1** and 64 ml dimethylsulfoxide (DMSO) under N_2. After the orange mixture was stirred for 5 min, 5.61 g (40 mmol) of *o*-Chlorobenzonitrile was added. The reaction was continued for 12 h at 130 ^{o}C. After this period, the mixture was pour into 600 ml of diluted hydrochloric acid and the generated mixture was extracted with diethyl ether. The combined golden yellow organic layers were dried with anhydrous

magnesium sulfate over night and then the solvent was evaporated. The obtained residue was purified on a short-column chromatography (silica gel, petroleum ether : ethyl acetate = 50 : 1), a light yellow microcrystalline solid was obtained (9.26 g, 89.4 %). ^{1}H NMR (400 MHz, $CDCl_3$) δ(ppm): 7.64-7.59 (m, 3H), 7.39-7.34 (m, 4H), 7.31-7.26 (m, 2H).

Synthesis of (2-(phenylselanyl)phenyl)methanamine (3). This compound was prepared according to a slight modification of the literature procedure[10]. A solution of 2-(phenylselanyl)benzonitrile **2** (2.58 g, 100 mmol) in 15ml tetrahydrofuran (THF) purified with sodium was added to a cooled lithium aluminium hydride (0.44 g, 12 mmol) in 10 ml THF. The reaction was stirred for 45 h at room temperature, and after there was no 2-(phenylselanyl)benzonitrile **2** in the reaction mixture, the reaction was quenched with 4 ml of water. The generated mixture was neutralized with 0.1 ml of 20 % sodium hydroxide aqueous solution. After of which, the mixture was filtered and the precipitate was washed with dichloromethane. Then the combined filtrates were dried over anhydrous magnesium sulfate and the solvent was evaporated on a rotary evaporator. The residue was purified on a short-column chromatography (silica gel, dichloromethane : ethanol = 30:1, + 1 % triethylamine), a yellow viscous liquid was obtained (1.64 g, 62.6 %). ^{1}H NMR (400 MHz, $CDCl_3$) δ(ppm): 7.42-7.12 (m, 9H), 3.95 (s, 2H), 1.64 (br, 2H). APCI-MS: m/z $C_{13}H_{13}NSe$ Calcd 263.0, found [M+H] 264.0.

Synthesis of *N*-butyl-4-bromo-1,8-naphthalimide (4). This compound was prepared according to a slight modification of the literature procedure[11]. 6 ml of n-butylamine in 50 ml ethanol was added to a 250 ml three-neck flask that containing 10 g (36 mmol) of 4-bromo-1,8-naphthalic anhydride in 150 ethanol and the mixture was refluxed for 1.5 h. After cooling to room temperature, the mixture was filtered and the precipitate was washed with ethyl acetate. The combined filtrates were evaporated and the acquired residue was purified on a short-column chromatography (silica gel, petroleum ether : ethyl acetate = 30 : 1), a white flocculent solid was gained (6.32 g, 52.7 %). ^{1}H NMR (400 MHz, $CDCl_3$) δ(ppm): 8.66-8.64 (m, 1H), 8.57-8.55 (m, 1H), 8.41 (d, J=8.0, 1H), 8.04 (d, J=8.0, 1H), 7.86-7.82 (m, 1H), 4.17 (t, J=6.0, 2H), 1.74-1.68 (m, 2H), 1.48-1.42 (m, 2H), 0.98 (t, J=8.0, 3H).

Synthesis of NI-Se. This compound was prepared according to a slight modification of the literature procedure[12]. Under the nitrogen atmosphere, 0.42 g (1.6 mmol) of (2-(phenylselanyl)phenyl)methanamine **3** and 0.43 g (1.3 mmol) of *N*-butyl-4-bromo-1,8-naphthalimide **4** were dissolved in 10 ml of 2-methoxyethanol. Then the solution was heated at 130 ^{o}C for 35 h and the solvent was evaporated. The residue was purified on a short-column chromatography (silica gel, dichloromethane), a yellow solid was obtained (0.22 g, 32.9 %). ^{1}H NMR (400 MHz, DMSO-D^6) δ(ppm): 8.78-8.73 (m, 1H), 8.45 (d, J=1.6 Hz, 1H), 8.18-8.09 (m, 1H), 7.72 (t, J=4.0, 1H), 7.50-7.24 (m, 9H), 6.68-6.39 (m, 1H), 5.75 (br, 1H), 4.68 (d, J=3.2, 2H), 4.00 (t, J=4.0 Hz, 2H), 1.60-1.55(m, 2H), 1.36-1.29(m, 2H), 0.91 (t, J=4.0 Hz, 3H). ^{13}C NMR (DMSO-D^6, 400 MHz) δ(ppm): 163.61, 162.79, 149.95, 139.28, 138.36, 134.94, 133.74, 132.11, 130.62, 130.42, 129.79, 128.72, 129.21, 128.51, 128.42, 128.29, 127.54, 127.48, 126.85, 124.43, 121.92, 120.25, 108.51, 104.35, 54.82, 46.53, 29.73, 19.73, 13.65. ^{77}Se NMR (DMSO-D^6, 400 MHz) δ(ppm): 360.60. HRMS: m/z $C_{29}H_{26}N_2O_2Se$ Calcd 514.1159, found 514.1149.

Synthesis of NI-SeO. 0.0205 g NI-Se was dissolved in 150 ml DMF, then 100 ml water and 40 ml 0.2 M PB was added into the solution. 200 ml 5.0×10^{-3} M NaOCl was added into the homogeneous solution, and the resulted mixture was stirred 30 min. The mixture was extracted with dichloromethane. The combined golden yellow organic layers were dried with anhydrous magnesium sulfate over night and then the solvent was evaporated. A yellow residue was obtained and used for further spectra measurements. ^{77}Se NMR (DMSO-D^6, 400 MHz) δ(ppm): 845.30. HRMS: m/z $C_{29}H_{26}N_2O_3Se$ Calcd 530.1109, found [M+H] 531.1146.

3. The TDDFT calculations of NI-Se

The frontier molecular orbitals of NI-Se and NI-SeO and the energy profiles were shown in Figure S1. It's clear that the energy level of donor orbital is lower than that of the accept orbital both in NI-Se and NI-SeO. This result demonstrates that there is no PET process in NI-Se or NI-SeO. The relevant calculated electronic transitions energies of NI–Se and NI–SeO at optimized geometries and the experimental results were shown in Table S1.

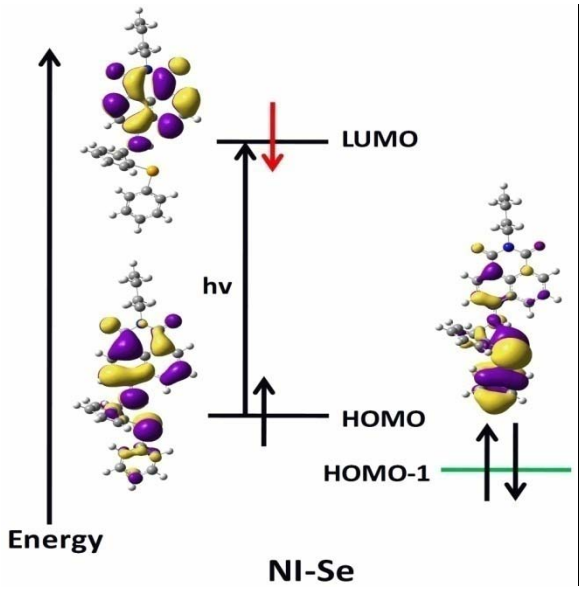

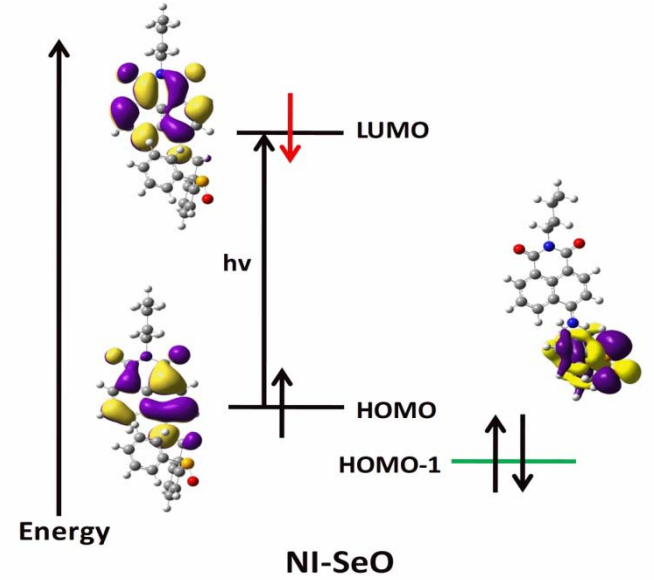

Figure S1. Frontier molecular orbital energy illustrations show the relative energetic dispositions of the orbitals of NI-Se and NI-SeO.

geometry	λ_{cal} (nm) [a]	λ_{exp} (nm) [b]	f [c]	CI expansion coefficients [d]
NI–Se				
S_0–S_1	434	450	0.378	98 % (HOMO → LUMO)
NI–SeO				
S_0–S_1	427	433	0.378	98 % (HOMO → LUMO)

[a]Calculated excitation wavelength. [b]Experimental absorption wavelength. [c]Oscillator strength. [d]Only the main contributions of each transition and their relevant MOs are listed.

Table S1. Vertical excited energies of NI–Se and NI–SeO at their optimized ground state geometries calculated at the TD–DFT/B3LYP/TZVP level.

4. The Influences of Viscosity and Temperature on Fluorescence Spectra

The influences of viscosity and temperature on the emission spectra of NI-Se and NI-SeO are shown in Figure S2. The fluorescence intensity of NI–Se increased gradually with increasing environmental viscosity (glycerol percent in ethanol), and was stronger at 77 K (the rotation of molecule was frozen) than that at 298 K (Figure S2a and S2c). The fluorescence of NI–SeO, however, was independent of neither viscosity nor temperature (Figure S2b and S2d). These results confirmed the twisting–induced fluorescence quenching mechanism of NI–Se, selenium oxidation blocked the twisting and the fluorescence was restored.

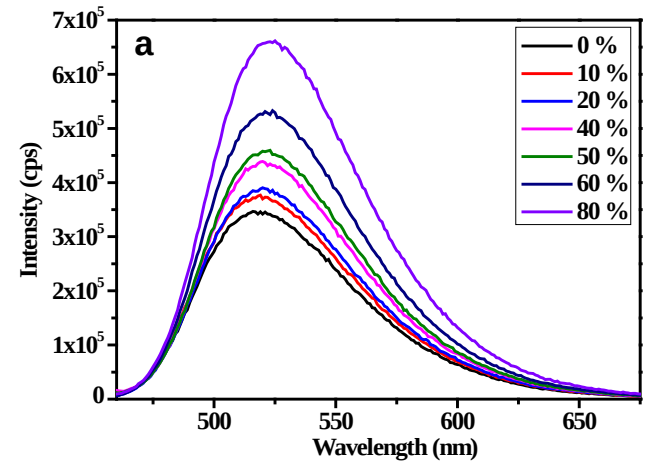

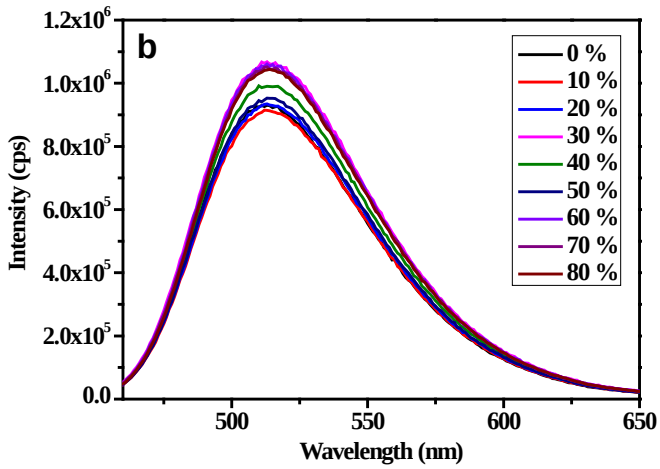

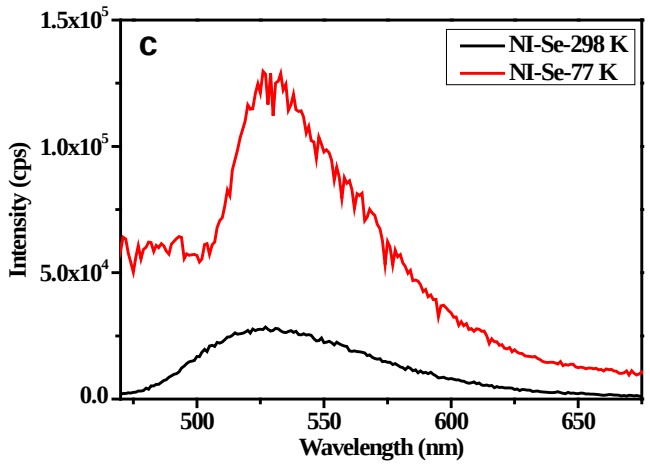

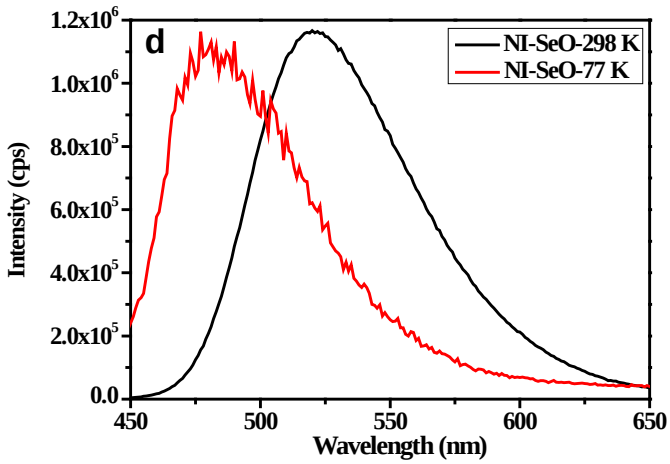

Figure S2. (a)The fluorescence spectra of compound **NI-Se** (3.0 μM) in ethanol upon the addition of glycerin. The fluorescence intensity was measured with the excitation wavelength 450 nm, and the excitation and emission slits set to 2 and 1 nm, respectively. (b) The fluorescence spectra of compound **NI-SeO** in ethanol upon the addition of glycerin. (c) Influences of temperature on the fluorescence spectra of NI-Se, the excitation and emission slits set to 2 and 1 nm, respectively. (d) Influences of temperature on the fluorescence spectra of NI-SeO, the excitation wavelength was set to be 420 nm.

5. Fluorescence Photographs of NI-Se Solution

The photographs of NI-Se solution in the absence and presence of sodium hypochlorite (NaOCl) at pH=7.40 were shown in Figure S3, which clearly demonstrated the increase of fluorescence intensity after the addition of NaClO.

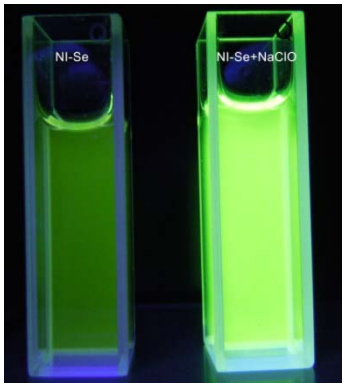

Figure S3. The fluorescence photographs of NI-Se in the absence (Left) and presence (Right) of NaOCl with the excitation of ultraviolet lamp (365 nm).

6. Absorption and Fluorescence Titration Experiment

The absorption and fluorescence titration spectra of NI-Se upon addition of

NaClO with different concentrations at pH=7.40 were performed. The absorption spectra with variety concentrations of NaOCl were shown in Figure S4a. The changes of fluorescence intensity at 523 nm dependent on the NaOCl concentrations were shown in Figure S4b,c.

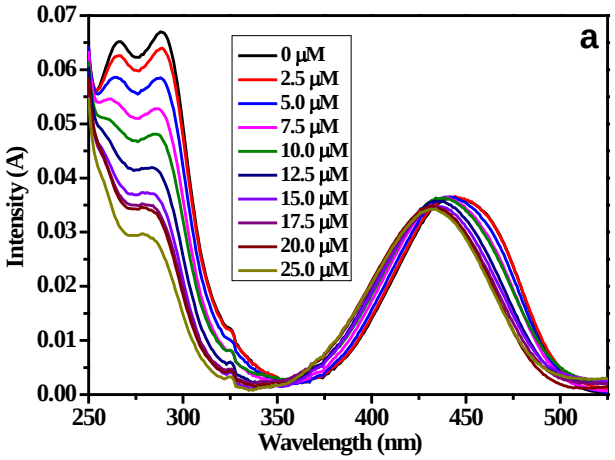

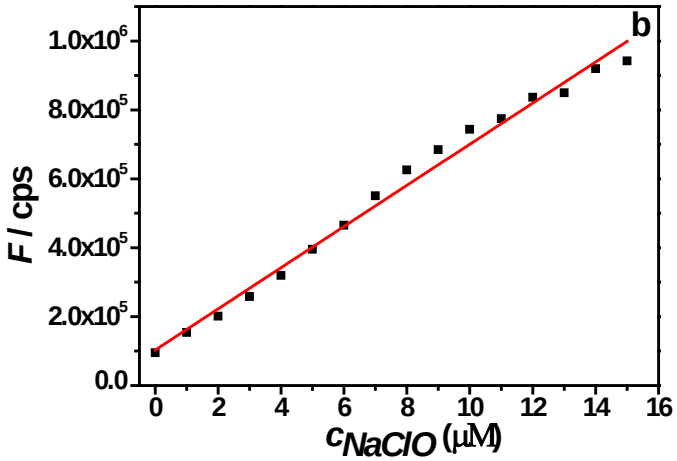

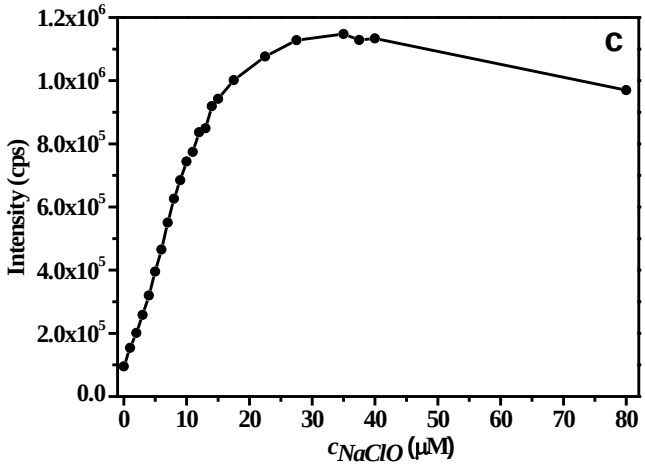

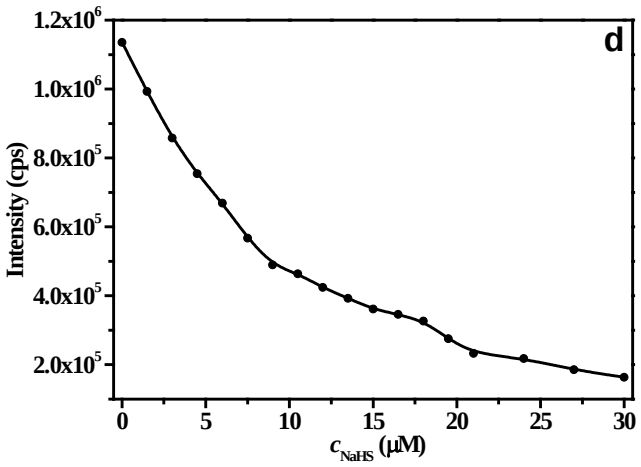

Figure S4. (a) Absorbance spectra of 3.0 μM NI-Se treated with various amounts of NaOCl. (b) Relationship between the fluorescence intensity at 523 nm and [NaOCl] (0-15 μM). (c) Fluorescence intensity of NI-Se at 523 nm responding to different concentrations of NaOCl (0, 1.0, 2.0, 3.0, 4.0, 5.0, 6.0, 7.0, 8.0, 9.0, 10.0, 11.0, 12.0, 13.0, 14.0, 15.0, 17.5, 22.5, 27.5, 35.0, 37.5, 40.0 and 100.0 μM). (d) Fluorescence intensity of NI-SeO at 521 nm responding to different concentrations of NaHS (0, 1.5, 3.0, 4.5, 6.0, 7.5, 9.0, 10.5, 12.0, 13.5, 15.0, 16.5, 18.0, 19.5, 21.0, 24.0, 27.0 and 30.0 μM).

7. The calculation of limit of detection

The detection limit was determined from the fluorescence titration data based on a reported method[13]. According to the result of titrating experiment, the fluorescence intensity at 523 nm were normalized between the minimum intensity and the maximum intensity. A linear regression curve was then fitted to these normalized fluorescence intensity data, and the point at which this line crossed the ordinate axis was considered as the detection limit (5.86×10^{-7} M).

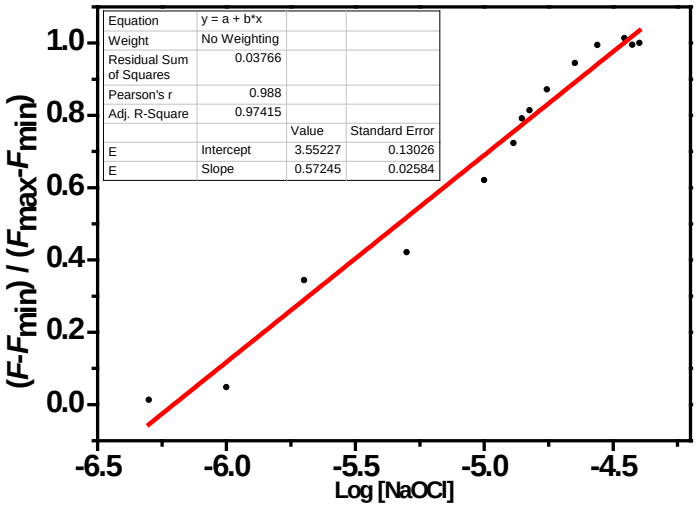

Figure S5. Normalized response of the fluorescence signal to changing NaOCl concentrations. Where, F_{max} was the maximum fluorescence intensity, F_{min} was the minimum fluorescence intensity, F was the fluorescence intensity at different NaOCl concentrations.

8. The Effects of pH values

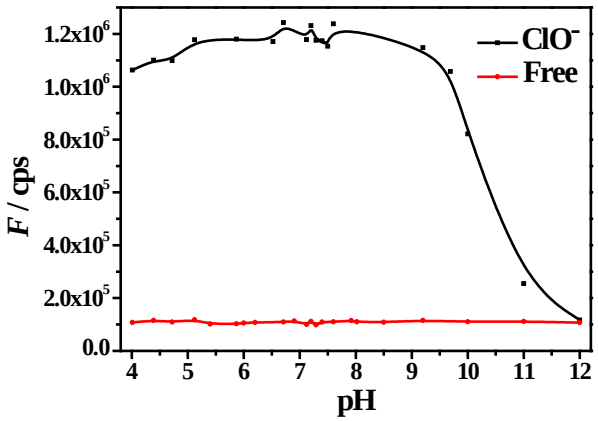

Figure S6. pH-dependent fluorescence intensity of NI-Se at 523 nm in the absence (circle, red) and presence (square, black) of NaOCl; the concentration of NaOCl was 30.0 μM.

9. The Selectivity of NI-Se

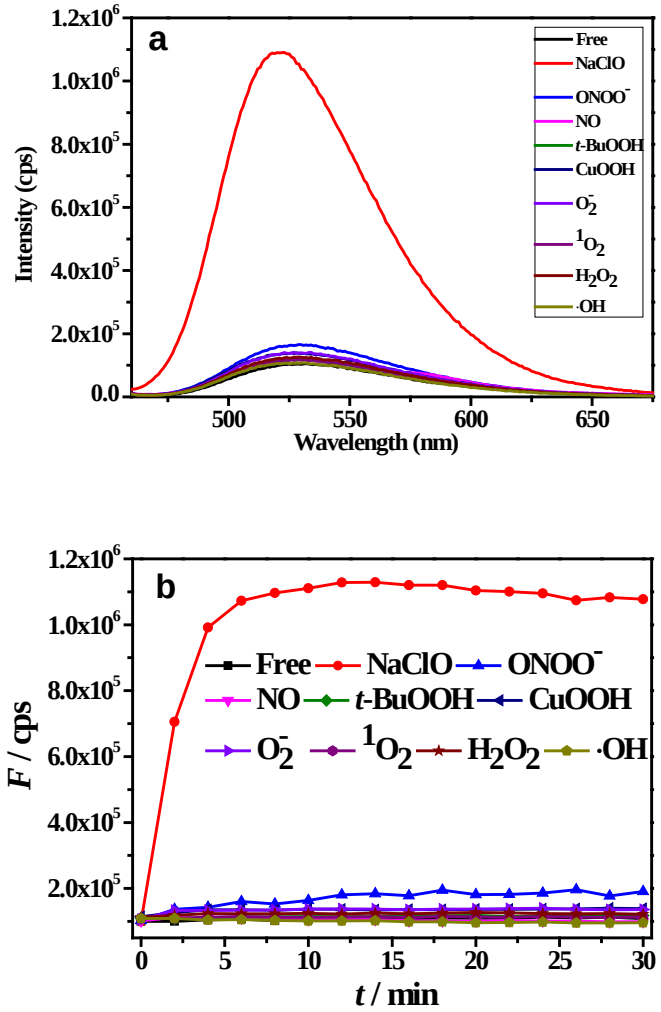

Figure S7. (a) The fluorescence spectra of NI-Se after addition of different ROS. The spectra were acquired equilibrated for 8 min after the addition of ROS. (b) Time course of NI-Se with each ROS for 30 min: 1, Free; 2, NaOCl (30.0 μM); 3, peroxynitrite (300.0 μM); 4, NO (150 μM); 5, tert-butylhydroperoxide (300.0 μM); 6, cumene hydroperoxide (300.0 μM); 7, O_2^-(300.0 μM); 8, $^1O_2$ (300.0 μM); 9, H_2O_2 (300.0 μM); 10, ·OH (300.0 μM).

10. Reversibility assays

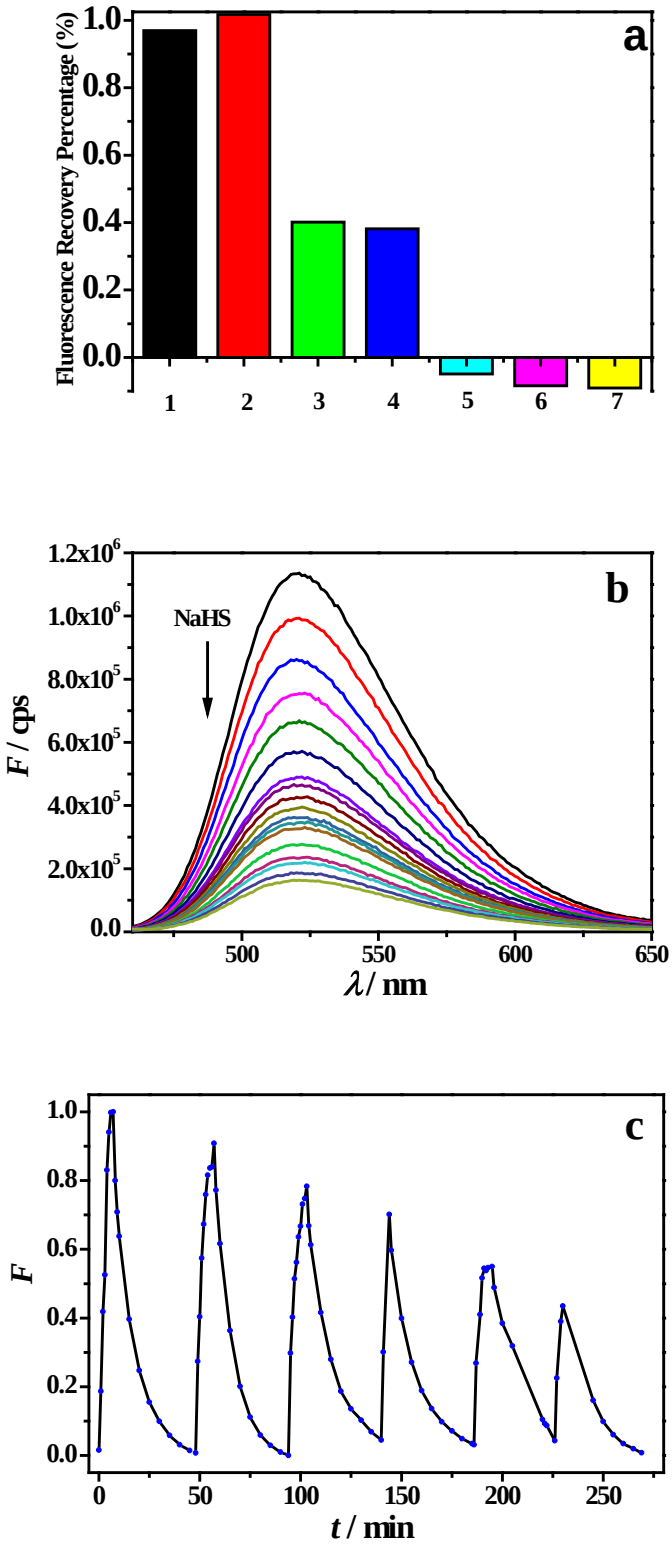

Figure S8. (a) Fluorescence recovery rate of various reducing materials. NI–Se was oxidized with 5 equiv of NaOCl. The solution was then treated with various reducing

compounds: 1, NaHS (60.0 μM); 2, Glutathione (3.0 mM); 3, Dithiothreitol (60 μM); 4, Cysteine (60 μM); 5, α-lipoic acid (60.0 μM); 6, Vitamin C (60.0 μM); 7, Histidine (60.0 μM). The fluorescence recovery rate (%) was calculated as follows: Fluorescence Recovery Rate $=(F_1-F)/(F_1-F_0) \times 100\%$, where F_1 is the fluorescence intensity after adding NaOCl, F is the fluorescence intensity of the probe after adding the reducing materials for 40 min, and F_0 is the initial fluorescence intensity of NI–Se in the absence of any substrate. All fluorescence intensities were acquired at 523 nm. (b) Changes in the fluorescence spectra of NI–SeO with different concentrations of NaHS. (c) Fluorescence responses of NI–Se to redox cycles. NI–Se was oxidized by 5 equiv of NaOCl. The solution was then treated with 20 equiv of NaHS after 8 min. Another 50 equiv of NaOCl was added when fluorescence returned to baseline levels. Subsequently, 20 equiv of NaHS was added to the mixture after another 8 min.

11. HPLC analysis of the redox cycles of NI-Se

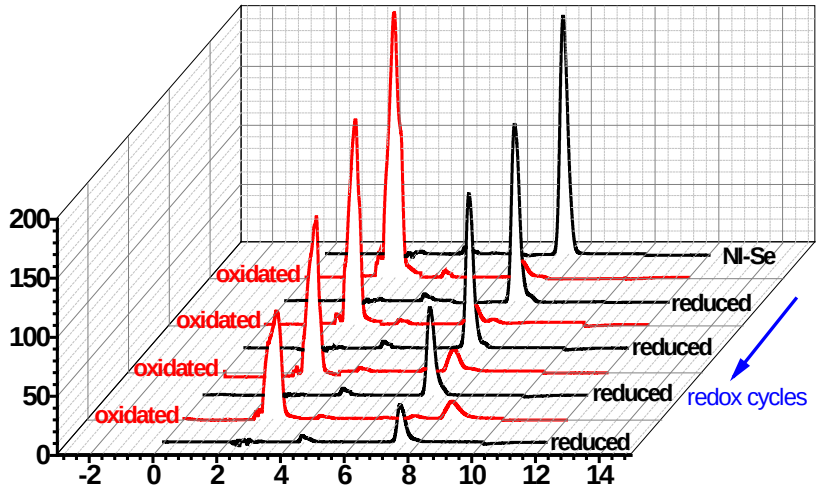

Figure S9. Monitoring the redox cycles of NI-Se between NaOCl and NaHS by HPLC analyses. NI-Se eluted at 7.1 min, NI-SeO eluted at 2.8 min with acetonitrile:water = 95 : 5 using UV-Vis detector at 450 nm and 254 nm, respectively.

12. MTT assay

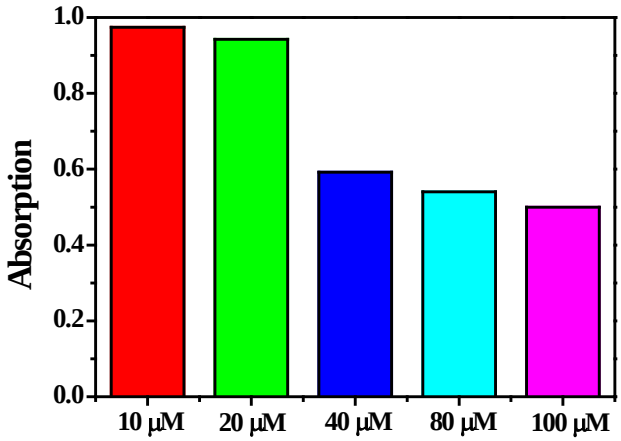

Figure S10. Cellular viability of RAW264.7 cells incubated with varying concentrations of NI-Se for 24 h. Viability of the cells was assessed using MTT assay. Percent viability was determined relative to the control group incubated with NI-Se solvent.

13. The solvent effect on fluorescent spectra of NI-Se

The fluorescent spectra of NI-Se in different solvents is shown in Figure S11. It can be noted that the fluorescence emission of NI-Se decreased with the increasing of the solvent polarity.

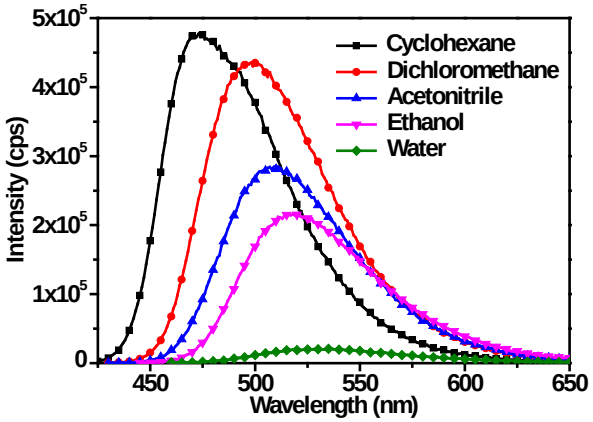

Figure S11. The fluorescent spectra of NI-Se (3.0 μM) in different solutions. The excitation and emission slits set to 2 and 1 nm, respectively.

14. The effect of BSA on fluorescent spectra of NI-Se

To investigate the influence of albumin or other small molecule binding protein which

exists in vivo, we examine the effect of BSA on the fluorescent spectra of NI-Se. It can be noted from Figure S12 that NI-Se can still monitor NaOCl screening to BSA, although the fluorescence intensity of NI-Se increased with the increasing of the concentrations of BSA. Consequently, we think the probe is capable of monitoring HOCl in living systems.

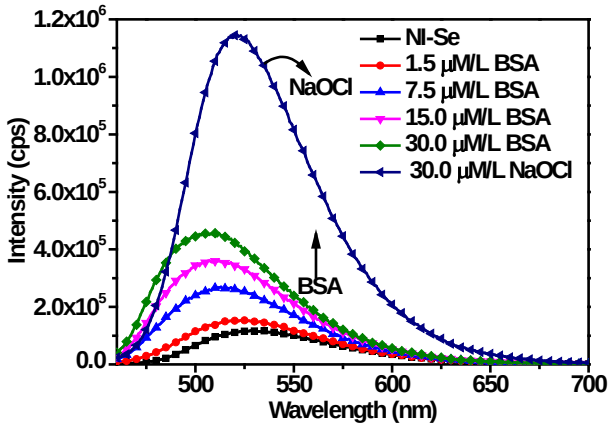

Figure S12. The fluorescent spectra of NI-Se (3.0 μM) with the increasing concentrations of BSA in PBS. The mixture was equilibrated for 8 min before measurement.

15. Additional fluorescent confocal images

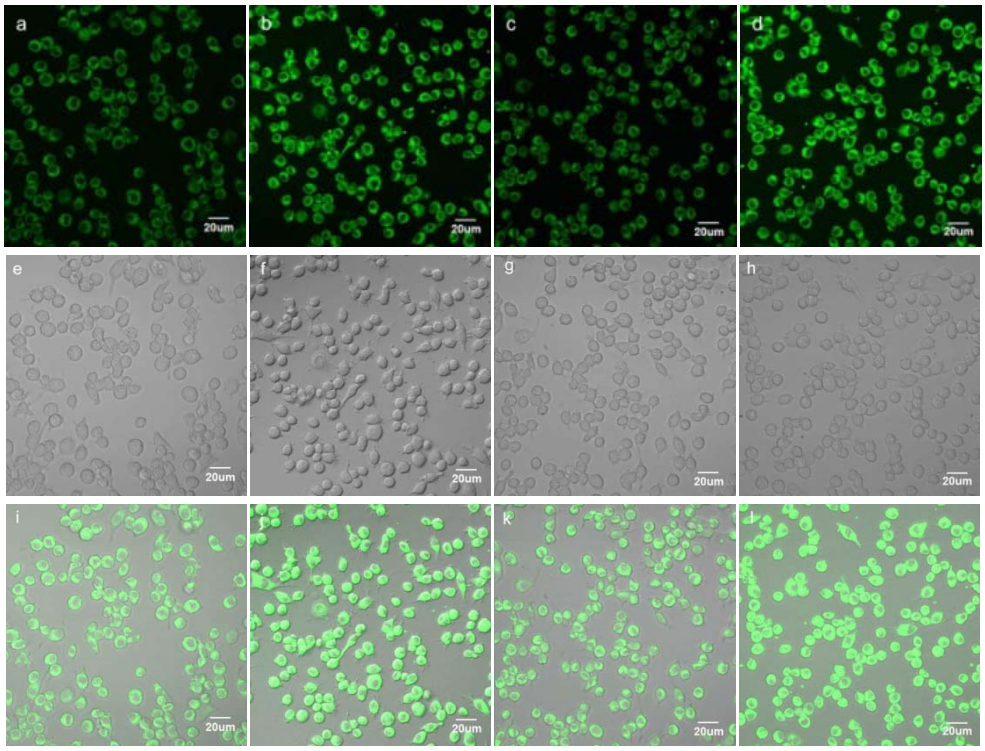

Figure S13. Confocal fluorescence images of HOCl and the reducing repair in living RAW264.7 cells. RAW264.7 cells were pretreated with 1 μg/mL LPS for 16 h. (a)

Incubated with 10 μM NI-Se for 5 min. (b) Incubated with 10 μM NI-Se for 5 min, and then stimulated with 2.5 μg/mL PMA for 30 min. (c) Addition of 5 U/ml GST for 10 min parallel to (b). (d) Addition of another 5.0 μg/mL PMA for 30 min parallel to (c). (e)-(h) were the bright-field images of (a)–(d). Images (i), (j), (k), (l) were the overlay of images (a), (b), (c), (d) with the images (e), (f), (g), (h), respectively.

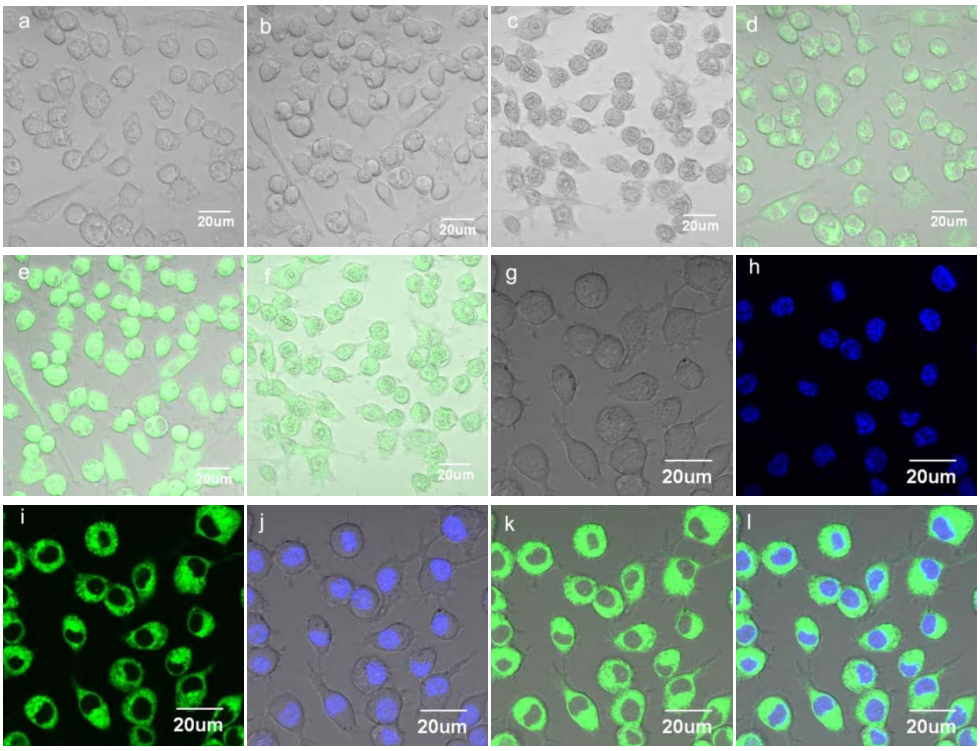

Figure S14. Bright-field images of Figure 3(a)–(c). Images (d)-(f) were the overlay of Figure 3(a)-(c) with the images (a)-(c), respectively. The images were obtained with an objective lens ×40. Image (g) was the bright field image of (i). (h) RAW264.7 cells loaded with 2 μM Hoechst 33342 and 10 μM NI-Se for 5 min, fluorescence image with a Hoechst 33342 dye filter set. (i) Fluorescence image with a NI-Se dye filter set of (h). Images (j), (k) were the overlay of (h), (i) with the image (g), respectively. Images (l) was the overlay of Figure 3d with the image (g). Images were obtained with an objective lens ×60.

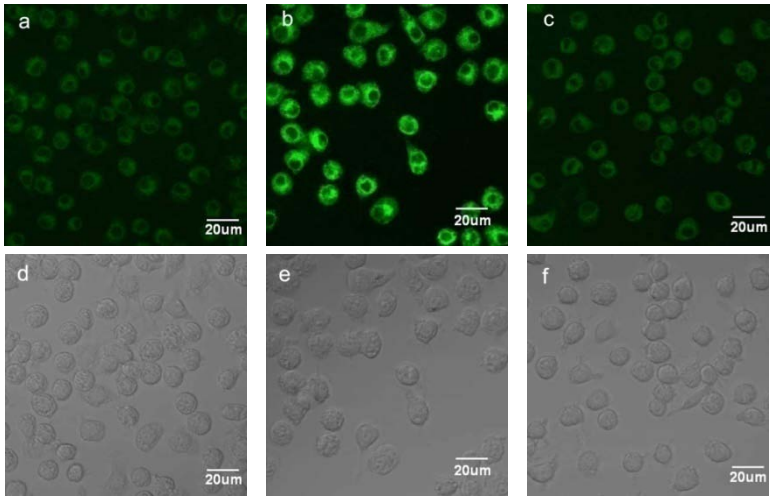

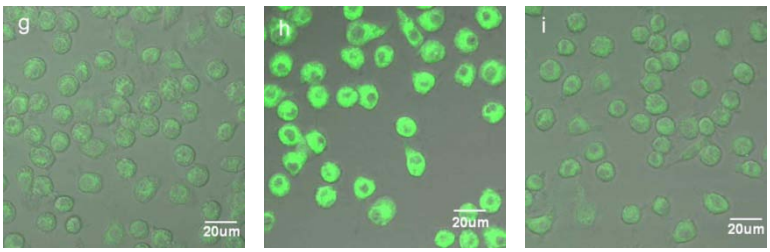

Figure S15. Confocal fluorescence images of the redox changes mediated by HOCl and the reducing repair in living RAW264.7 cells. RAW264.7 cells was pretreated with 1 μg/mL LPS for 16 h. (a) Only incubated with 10 μM NI-Se for 5 min. (b) Incubated with 10 μM NI-Se for 5 min then stimulated with 2.5 μg/mL PMA for 30 min. (c) Addition of 300 μM NaHS that in parallel to (b). Bright-field images of Figure a–c. Image (g), (h), (i) was the overlay of Figure (a), (b), (c) with the image (d), (e), (f), respectively.

16. Additional Spectroscopic Data

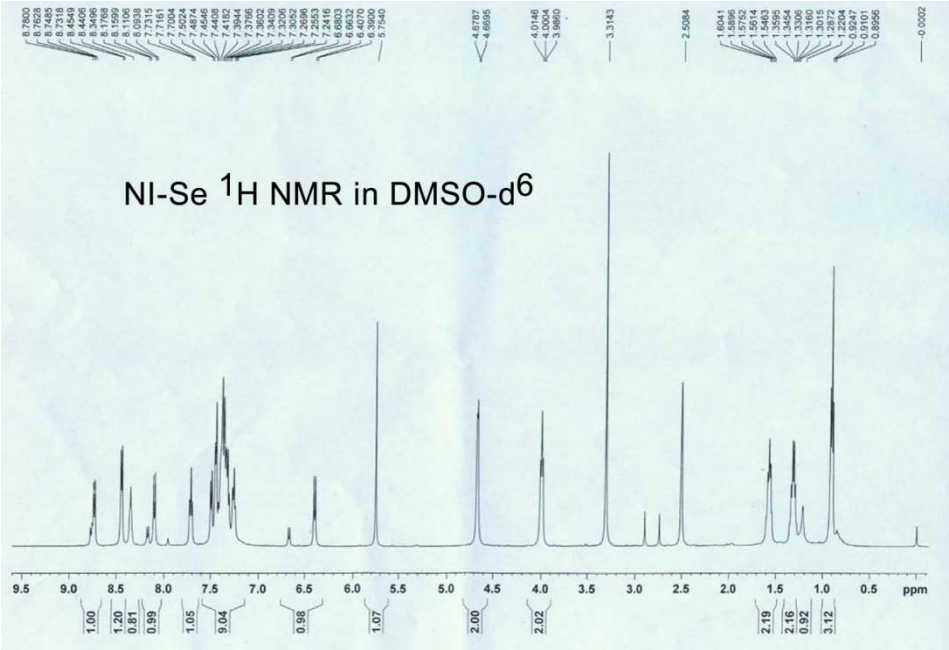

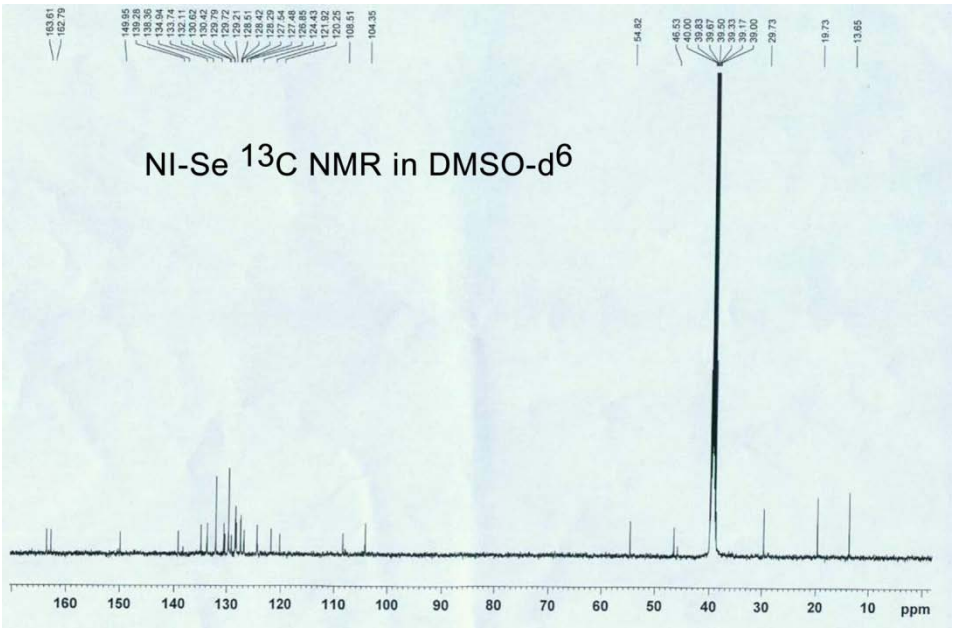
NI-Se 13C NMR in DMSO-d6
163.61
162.79
149.95
139.28
138.36
134.94
133.74
132.11
130.62
130.42
129.79
129.77
129.21
128.51
128.42
128.29
127.54
127.48
126.85
124.43
121.32
121.25
108.51
104.35
54.82
46.53
40.00
39.83
39.67
39.50
39.33
39.17
39.00
29.73
19.73
13.65
160 150 140 130 120 110 100 90 80 70 60 50 40 30 20 10 ppm

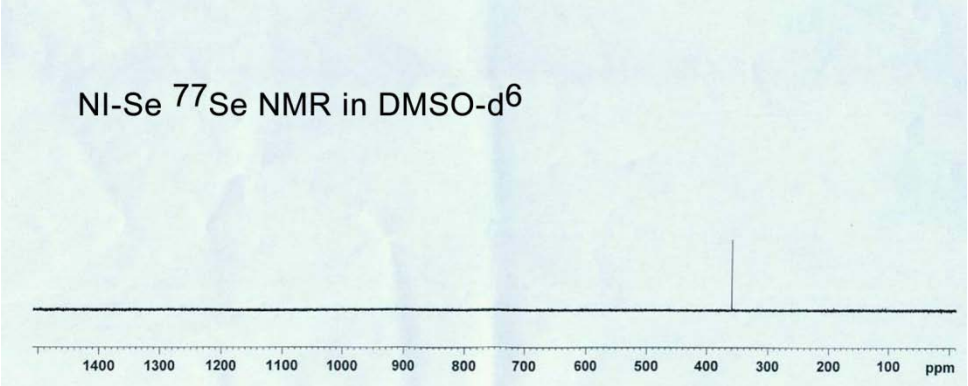
NI-Se 77Se NMR in DMSO-d6
1400 1300 1200 1100 1000 900 800 700 600 500 400 300 200 100 ppm

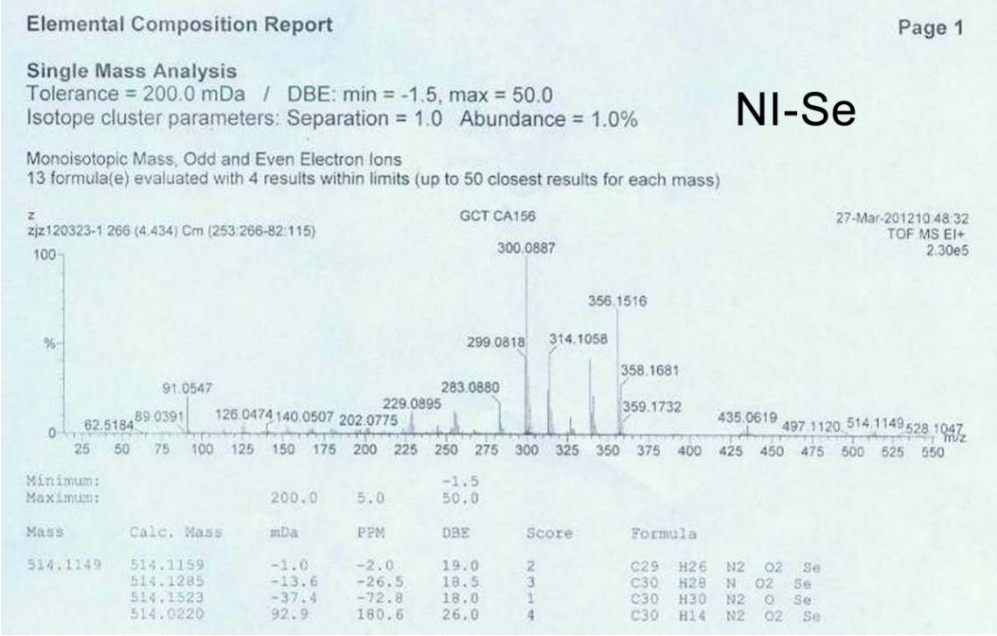
Elemental Composition Report
Page 1
Single Mass Analysis
Tolerance = 200.0 mDa / DBE: min = -1.5, max = 50.0
Isotope cluster parameters: Separation = 1.0 Abundance = 1.0%
NI-Se
Monoisotopic Mass, Odd and Even Electron Ions
13 formula(e) evaluated with 4 results within limits (up to 50 closest results for each mass)
z
zjz120323-1 266 (4.434) Cm (253:266-82:115)
GCT CA156
27-Mar-201210:48:32
TOF MS EI+
2.30e5
300.0887
356.1516
299.0818
314.1058
358.1681
91.0547
283.0880
229.0895
359.1732
62.5184
89.0391
126.0474
140.0507
202.0775
435.0619
497.1120
514.1149
528.1047
m/z
Minimum: -1.5
Maximum: 200.0 5.0 50.0
Mass Calc. Mass mDa PPM DBE Score Formula
514.1149 514.1159 -1.0 -2.0 19.0 2 C29 H26 N2 O2 Se
514.1285 -13.6 -26.5 18.5 3 C30 H28 N O2 Se
514.1523 -37.4 -72.8 18.0 1 C30 H30 N2 O Se
514.0220 92.9 180.6 26.0 4 C30 H14 N2 O2 Se

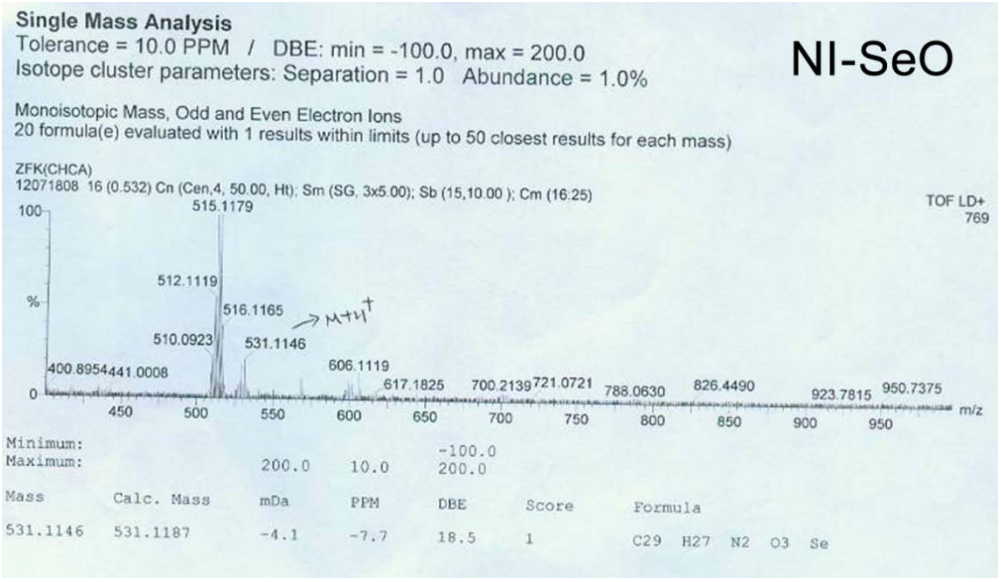

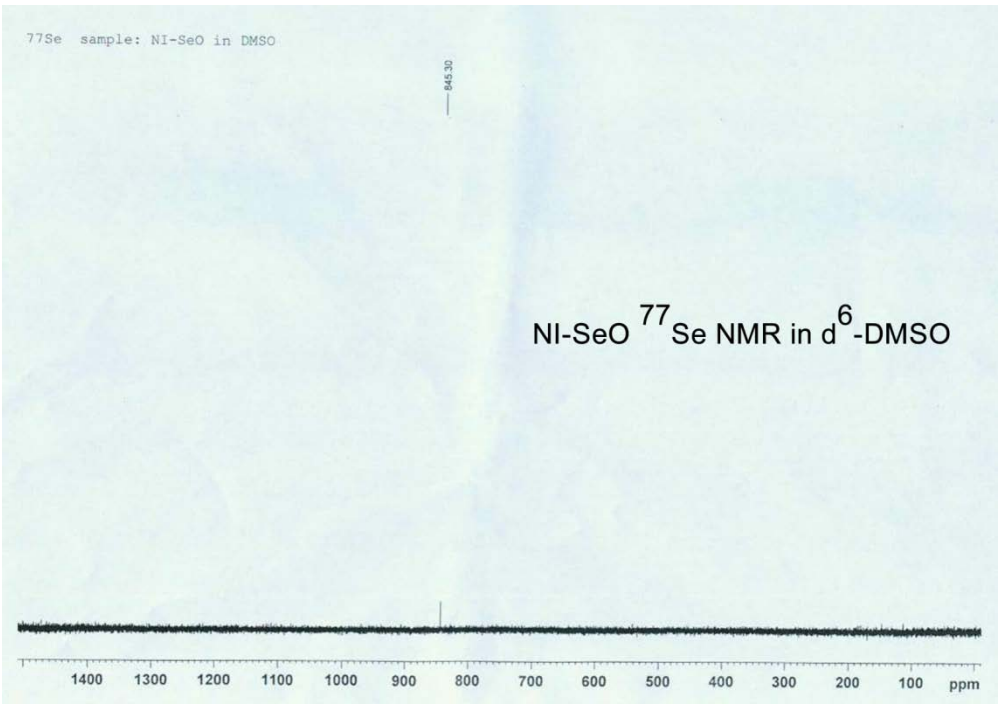

17. References

[1] Ashki, N.; Hayes, K. C.; Bao, F. *Neuroscience* **2008**, *156*, 107.
[2] Free Radicals in Biology and Medicine. New York, Oxford University Press, 1989, 58.
[3] Albers A. E.; Okreglak V. S.; Chang C. J. *Journal of the American Chemical Society* **2006**, *128*, 9640.
[4] Halliwell B.; Gutteridge J. M. C.; *Archives of Biochemistry and Biophysics* **1986**, *246*, 501.
[5] Nieminen, A. L.; Byrne, A. M.; Herman B.; Lemasters, J. *American Journal of Physiology-Cell Physiology* **1997**, *272*, 1286.

[6] Morris J. C. *The Journal of Physical Chemistry* **1966**, *70*, 3798.
[7] Gaussian 09, Revision A.02, Frisch, M. J.; Trucks, G. W.; Schlegel, H. B.; Scuseria, G. E.; Robb, M. A.; Cheeseman, J. R.; Scalmani, G.; Barone, V.; Mennucci, B.; Petersson, G. A.; Nakatsuji, H.; Caricato, M.; Li, X.; Hratchian, H. P.; Izmaylov, A. F.; Bloino, J.; Zheng, G.; Sonnenberg, J. L.; Hada, M.; Ehara, M.; Toyota, K.; Fukuda, R.; Hasegawa, J.; Ishida, M.; Nakajima, T.; Honda, Y.; Kitao, O.; Nakai, H.; Vreven, T.; Montgomery, J. A., Jr.; Peralta, J. E.; Ogliaro, F.; Bearpark, M.; Heyd, J. J.; Brothers, E.; Kudin, K. N.; Staroverov, V. N.; Kobayashi, R.; Normand, J.; Raghavachari, K.; Rendell, A.; Burant, J. C.; Iyengar, S. S.; Tomasi, J.; Cossi, M.; Rega, N.; Millam, N. J.; Klene, M.; Knox, J. E.; Cross, J. B.; Bakken, V.; Adamo, C.; Jaramillo, J.; Gomperts, R.; Stratmann, R. E.; Yazyev, O.; Austin, A. J.; Cammi, R.; Pomelli, C.; Ochterski, J. W.; Martin, R. L.; Morok ma, K.; Zakrzewski, V. G.; Voth, G. A.; Salvador, P.; Dannenberg, J. J.; Dapprich, S.; Daniels, A. D.; Farkas, O.; Foresman, J. B.; Ortiz, J. V.; Cioslowski, J.; Fox, D. J. Gaussian 09, Revision A.02; Gaussian, Inc.: Wallingford, CT, 2009.
[8] Reich, H. J.; Cohen, M. L.; Clark, P. S. *Organic Syntheses* **1988**, *50*, 533.
[9] Henriksen, L.; Stuhr-Hansen, N. *Journal of the Chemical Society-Perkin Transactions 1*, **1999**, 1915.
[10] Soffer, L. M.; Katz, M. *Journal of the American Chemical Society* **1956**, 78, 1705.
[11] Yang, P.; Yang, Q.; Qian, X. *Tetrahedron* **2005**, 61, 11895.
[12] Xu, Z.; Xiao, Y.; Qian, X.; Cui, J.; Cui, D. *Orgnic Letter* **2005**, 7, 889.
[13] M. Shortreed, R. Kopelman, M. Kuhn and B. Hoyland, *Anal. Chem.*, 1996, **68**, 1414-1418.